



An explicit hybrid finite difference scheme for the Allen–Cahn equation

Darae Jeong, Junseok Kim*

Department of Mathematics, Korea University, Seoul 136-713, Republic of Korea



HIGHLIGHTS

- We propose an explicit hybrid numerical method for solving the Allen–Cahn equation.
- The proposed method is based on an operator splitting method.
- We show the stability condition of the proposed numerical scheme.
- We show the pointwise boundedness of the solution under a solvability condition.

ARTICLE INFO

Article history:

Received 6 April 2016

Received in revised form 25 October 2017

Keywords:

Allen–Cahn equation

Finite difference method

Explicit hybrid method

Operator splitting method

ABSTRACT

In this paper, we propose an explicit hybrid numerical method for solving the Allen–Cahn equation, which models antiphase domain coarsening process in a binary mixture. The proposed method is based on an operator splitting method. First, we solve the linear diffusion part using the explicit Euler method. Second, we solve the nonlinear term using the closed-form analytical solution. We show the stability condition of the proposed numerical scheme. We also show the pointwise boundedness of the numerical solution for the Allen–Cahn equation under a solvability condition. Numerical experiments such as linear stability analysis, traveling wave, motion by mean curvature, image segmentation, and crystal growth are presented to demonstrate the performance of the proposed method.

© 2018 Elsevier B.V. All rights reserved.

1. Introduction

In this paper, we propose an explicit hybrid numerical method for solving the Allen–Cahn (AC) equation [1]:

$$\begin{aligned} \frac{\partial \phi(\mathbf{x}, t)}{\partial t} &= -\frac{F'(\phi(\mathbf{x}, t))}{\epsilon^2} + \Delta \phi(\mathbf{x}, t), \quad \mathbf{x} \in \Omega, \quad t > 0, \\ \mathbf{n} \cdot \nabla \phi(\mathbf{x}, t) &= 0 \text{ on } \partial \Omega, \end{aligned} \quad (1)$$

where $\Omega \subset \mathbb{R}^d$ ($d = 1, 2, 3$) is a domain with outer unit normal vector \mathbf{n} . Here, $\phi(\mathbf{x}, t)$ is the difference between the concentrations of the two mixtures' components, $F(\phi) = 0.25(\phi^2 - 1)^2$, and ϵ is a positive constant. The AC equation was originally introduced as a mathematical model for antiphase domain coarsening in a binary alloy and is the L^2 -gradient flow of the following total free energy functional:

$$\mathcal{E}(\phi) = \int_{\Omega} \left(\frac{F(\phi)}{\epsilon^2} + \frac{1}{2} |\nabla \phi|^2 \right) dx.$$

* Corresponding author.

E-mail address: cfdkim@korea.ac.kr (J. Kim).

URL: <http://math.korea.ac.kr/~cfdkim/> (J. Kim).

The AC equation has been successfully used to model a class of problems such as crystal growth [2], image inpainting [3], image segmentation [4,5], mean curvature flows [6,7], and the mixture of two incompressible fluids [8,9] to name just a few.

The AC equation is a nonlinear equation. Except some special cases, in general, the analytic solution is not available. Thus, we have to resort to numerical methods to obtain an approximate solution. There have been many numerical methods developed to solve the AC equation (see e.g., [10–23] and the reference therein). Yang [24] considered stabilized semi-implicit splitting schemes. For the stabilized first-order scheme, Yang showed that it is unconditionally stable. An unconditionally gradient stable scheme [25] and a hybrid splitting scheme [26] were proposed. A first and a second order semi-analytical Fourier spectral methods for the Allen–Cahn equation were presented in [19]. A second-order operator splitting method for the AC equation with nonlinear source terms was proposed in [27]. The authors in [12] investigated the first- and second-order implicit–explicit schemes that inherit the nonlinear stability, the free-energy functional decreases in time, of the continuous model for solving the AC equation. The authors in [7] developed and analyzed two fully discrete interior penalty discontinuous Galerkin methods for the AC equation. An unconditionally stable hybrid finite element method for solving the Allen–Cahn equation was presented in [22]. In [28], an explicit numerical method and its fast implementation were proposed for the AC equation. The method combines decompositions of compact spatial difference operators with exponential time integrators and discrete FFT-based algorithms. Recently, Aderogba and Chapwanya [29] designed explicit nonstandard finite difference schemes for the nonlinear AC equation.

In the AC equation, we must solve a Poisson-type equation. Almost all previous stable numerical schemes are either implicit or semi-implicit. On the other hand, if we want to get an accurate numerical solution, we have to use a small enough time step. In these limits, it is better to use a fully explicit scheme. However, it has a severe time step restriction if we use the fully explicit scheme. In this paper, we propose an explicit hybrid numerical scheme for the AC equation, which has a practical stability. This paper is organized as follows. In Section 2, we describe numerical analysis such as solvability and the boundedness of the numerical solution. We present the numerical results for several examples in Section 3. In Section 4, we conclude.

2. Numerical solution and its analysis

We present an explicit hybrid numerical scheme for the AC equation. For simplicity, we discretize the AC equation in the one-dimensional space $\Omega = (a, b)$. Higher-dimensional discretizations are similarly defined. Let N be a positive integer, $h = (b - a)/N$ be the uniform mesh size, and $\Omega_h = \{x_i = a + (i - 0.5)h, 1 \leq i \leq N\}$ be the set of cell-centers. Let ϕ_i^n be approximations of $\phi(x_i, n\Delta t)$, where $\Delta t = T/N_t$ is the time step, T is the final time, and N_t is the total number of time steps. Let a discrete differentiation operator be $\nabla_h \phi_{i+1/2}^n = (\phi_{i+1}^n - \phi_i^n)/h$, then the zero Neumann boundary condition is defined as $\nabla_h \phi_{1/2}^n = \nabla_h \phi_{N+1/2}^n = 0$. We then define a discrete Laplacian by $\Delta_h \phi_i = (\nabla_h \phi_{i+1/2} - \nabla_h \phi_{i-1/2})/h$. We denote the discrete maximum norm by $\|\phi^n\|_\infty = \max_{1 \leq i \leq N} |\phi_i^n|$, where $\phi^n = (\phi_1^n, \phi_2^n, \dots, \phi_N^n)$.

2.1. Numerical algorithm of the proposed explicit hybrid scheme

The proposed explicit hybrid scheme consists of two steps as follows. First, we solve the following diffusion equation

$$\frac{\phi_i^* - \phi_i^n}{\Delta t} = \Delta_h \phi_i^n \text{ for } 1 \leq i \leq N, \tag{2}$$

and then we get $\phi_i^{n+1} = \psi(\Delta t)$ by analytically solving

$$\psi_t = \frac{\psi - \psi^3}{\epsilon^2} \text{ with the initial condition } \psi(0) = \phi_i^*.$$

That is,

$$\phi_i^{n+1} = \frac{\phi_i^*}{\sqrt{[1 - (\phi_i^*)^2]e^{-2\Delta t/\epsilon^2} + (\phi_i^*)^2}} \text{ for } 1 \leq i \leq N.$$

This scheme is explicit, therefore we do not need to solve a system of discrete equations and it is very fast. We note that if we use the forward Euler method for the nonlinear step, i.e.,

$$\phi_i^{n+1} = \phi_i^* + \frac{\Delta t}{\epsilon^2} [\phi_i^* - (\phi_i^*)^3],$$

then $|\phi_i^{n+1}| > 1$ for $\Delta t > \epsilon^2/[|\phi_i^*|(|\phi_i^*| + 1)]$, $\phi_i^* \neq 0$, and $|\phi_i^*| \neq 1$. Therefore, the forward Euler method requires that the time step size Δt should be $O(\epsilon^2)$.

2.2. Stability of the proposed explicit hybrid scheme

Solvability of the proposed scheme is trivial since it is explicitly well defined. By using the discrete von Neumann stability analysis, we have the stability condition for the first step, which is expressed as follows from Eq. (2):

$$\Delta t \leq 0.5h^2/d, \tag{3}$$

where d is the dimension of the computational space [30].

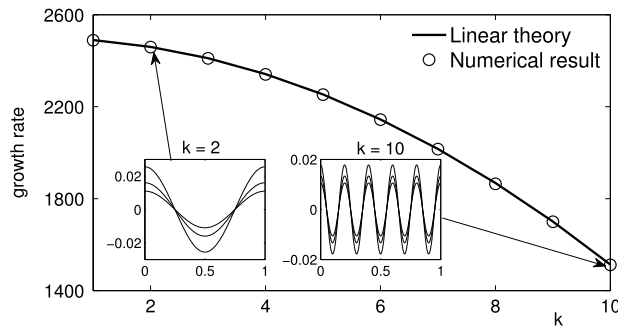


Fig. 1. Growth rates of numerical and exact solutions with respect to different wave numbers k . Inserted small figures illustrate temporal evolutions of numerical solution when $k = 2$ and $k = 10$.

2.3. Boundedness of the proposed explicit hybrid scheme

Let us assume $\|\phi^n\|_\infty \leq 1$ for some n . By the discrete maximum principle for the numerical solution of Eq. (2) under the stability condition (3), we have $\|\phi^*\|_\infty \leq 1$. If $\phi_i^* = 0$, then $\phi_i^{n+1} = 0$; otherwise, i.e., if $0 < |\phi_i^*| \leq 1$, then

$$|\phi_i^{n+1}| = \frac{1}{\sqrt{1 + ((\phi_i^*)^{-2} - 1)e^{-2\Delta t/\epsilon^2}}} \leq 1.$$

Therefore, if $\|\phi^0\|_\infty \leq 1$, then $\|\phi^n\|_\infty \leq 1$ for all $n = 1, 2, \dots$. We should note that the stability and boundedness of the proposed numerical scheme are independent of the value of ϵ .

3. Numerical experiments

In this section, we perform several numerical tests such as linear stability analysis, traveling wave, motion by mean curvature, image segmentation, and crystal growth. Before we start, we define the interfacial length parameter ϵ_m as follows.

$$\epsilon_m = mh/[2\sqrt{2}\tanh^{-1}(0.9)] \approx 0.24015mh,$$

which implies that we have approximately mh transition layer width [25]. For all tests, we use $\epsilon = \epsilon_m$ for some integer m , unless otherwise specified.

3.1. Linear stability analysis

We perform a linear stability analysis [25,31]. By linearizing the AC equation (1) around $\phi \equiv 0$, we have

$$\phi_t = \frac{\phi}{\epsilon^2} + \phi_{xx}. \tag{4}$$

If we assume $\phi(x, t) = \alpha(t) \cos(k\pi x)$, where k is a wave number, then we get the following from Eq. (4) as

$$\alpha'(t) \cos(k\pi x) = \frac{\alpha(t) \cos(k\pi x)}{\epsilon^2} - (k\pi)^2 \alpha(t) \cos(k\pi x).$$

Thus, $\alpha(t) = \alpha(0)e^{\lambda t}$, where $\lambda = 1/\epsilon^2 - (k\pi)^2$ is a growth rate. We also define the numerical growth rate by

$$\bar{\lambda} = \frac{1}{T} \log \left(\frac{\|\phi^{Nt}\|_\infty}{\alpha(0)} \right).$$

The initial data is given by $\phi(x, 0) = \alpha(0) \cos(k\pi x)$ on the computational domain $\Omega = (0, 1)$ with parameters $\epsilon = 0.02$, $N = 256$, $\alpha(0) = 0.01$, $\Delta t = 0.25h^2$, and the final time $T = 100\Delta t$.

Fig. 1 represents the linear stability test by the proposed scheme. As shown in Fig. 1, numerical result $\bar{\lambda}$ (circled markers) and exact result λ (solid line) for different wave numbers k ($k = 1, 2, \dots, 10$) are in good agreement.

3.2. Convergence of traveling wave solutions

One of the exact solutions of the AC equation is the traveling wave solution $\phi(x, t) = 0.5 - 0.5 \tanh[(x - 2 - st)/(2\sqrt{2}\epsilon)]$, where $s = 3/(\sqrt{2}\epsilon)$ is the speed of the traveling wave [25,32]. Now, we investigate the performance of the proposed numerical scheme on the traveling wave problem. For the numerical tests, we use the different spatial step sizes $h = h_0$,

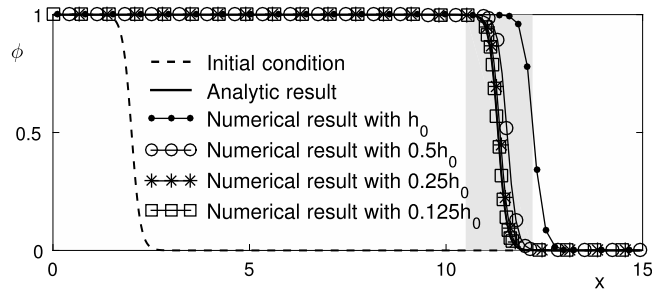


Fig. 2. Convergence of numerical traveling wave solutions at $t = T$ with an initial profile $\phi(x, 0) = 0.5 - 0.5 \tanh[(x - 2)/(2\sqrt{2}\epsilon)]$, where $\epsilon = 0.08$.

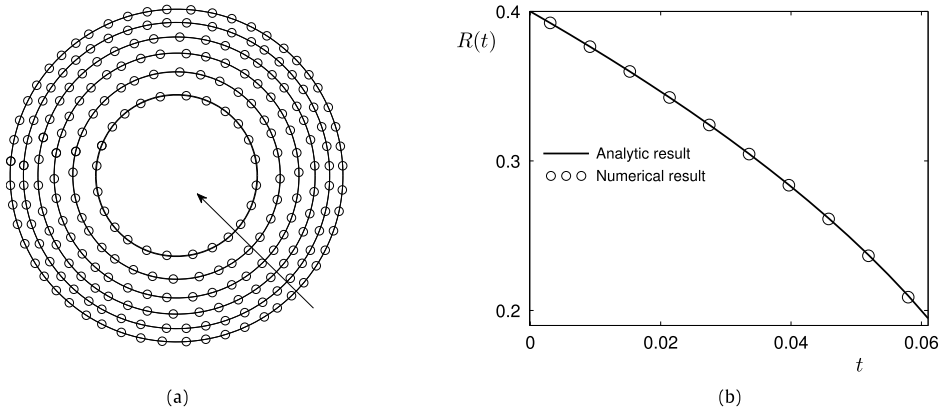


Fig. 3. Temporal evolutions of the radius with $\Delta t = 0.1h^2$ until $t = 250h^2$ in the two-dimensional space. (a) Zero level contours and (b) radius $R(t)$ of circle with respect to time. Here, arrow represents the direction of time evolution.

$0.5h_0$, $0.25h_0$, and $0.125h_0$ on $\Omega = (0, 15)$. Other parameters used are $h_0 = 15/64$, $\Delta t = 0.01h^2$, $T = 6.4h_0^2$, and $\epsilon = 0.08$. In Fig. 2, the dashed line shows the initial condition $\phi(x, 0) = 0.5 - 0.5 \tanh[(x - 2)/(2\sqrt{2}\epsilon)]$. Also, the analytic traveling wave solution at $t = T$ is represented by the solid line. On a set of increasingly finer grids and time steps, we obtain the convergence of the numerical solution to the exact solution.

3.3. Motion by mean curvature

It was formally proved that, as $\epsilon \rightarrow 0$, the zero level set of ϕ evolves according to the geometric law

$$V = -\kappa = -\left(\frac{1}{R_1} + \frac{1}{R_2}\right), \tag{5}$$

where V is the normal velocity of the surface at each point, κ is its mean curvature, and R_1, R_2 are the principal radii of curvatures at the point of the surface [1]. In the two-dimensional space, Eq. (5) becomes $V = -1/R$.

An initial condition is given as a circle with center $(0.5, 0.5)$ and radius $R_0 = 0.4$ on the computational domain $\Omega = (0, 1) \times (0, 1)$, that is,

$$\phi(x, y, 0) = \tanh \frac{R_0 - \sqrt{(x - 0.5)^2 + (y - 0.5)^2}}{\sqrt{2}\epsilon_8}.$$

Let R_0 and $R(t)$ be the initial radius and the radius at time t of the circle, respectively. Then Eq. (5) becomes $dR(t)/dt = -1/R(t)$. Therefore, analytic solution is given as $R(t) = \sqrt{R_0^2 - 2t}$. For the numerical test, we use $\epsilon_8, h = 1/64, \Delta t = 0.1h^2$, and $T = 250h^2$. Fig. 3(a) and (b) show the temporal evolution of the initial circle and its radius with respect to time. For verification of our numerical results, we include the results of the analytic solution. As shown in Fig. 3, the initial circle shrinks under the motion by mean curvature.

We also test the same simulation on the three-dimensional space $\Omega = (0, 1) \times (0, 1) \times (0, 1)$. The initial condition is given as

$$\phi(x, y, z, 0) = \tanh \frac{R_0 - \sqrt{(x - 0.5)^2 + (y - 0.5)^2 + (z - 0.5)^2}}{\sqrt{2}\epsilon_8}.$$

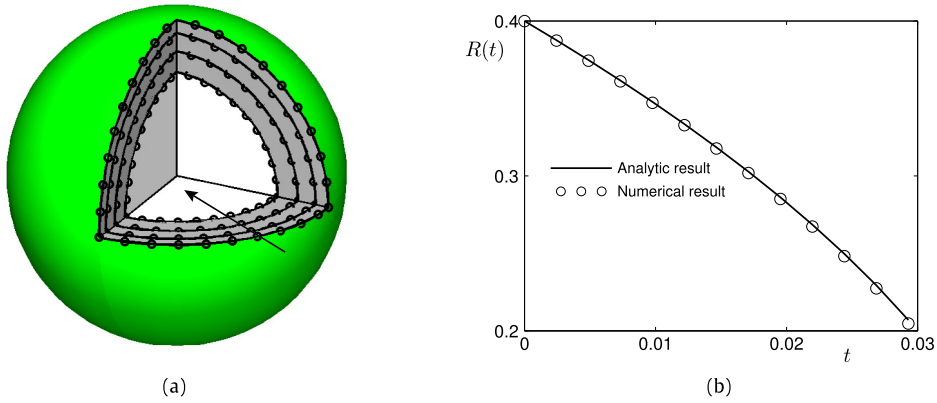


Fig. 4. Temporal evolutions of the radius with $\Delta t = 0.1h^2$ up to $t = 250h^2$ in the three-dimensional space. (a) Zero level isosurfaces and (b) radius $R(t)$ of sphere with respect to time. Here, arrow represents the direction of time evolution.

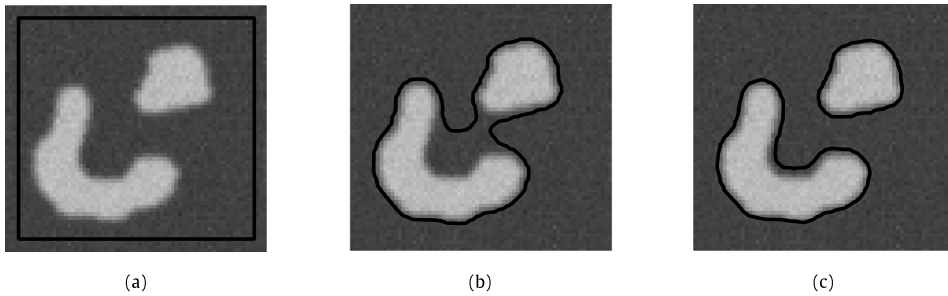


Fig. 5. Image segmentation process at (a) 0 iteration (b) 240 iterations, and (c) 400 iterations. Here, original image is reprinted from Ref. [33] with permission. Numerical parameters are used by $\sigma = 1.5$, $\beta = 5e4$, ϵ_8 , $h = 0.01$, $\Delta t = 0.2h^2$, and 71×67 mesh grid.

We use the same parameter values as the two-dimensional case except $T = 120h^2$. Fig. 4 illustrates temporal evolutions of the sphere with the analytic solution, which is defined by $R(t) = \sqrt{R_0^2 - 4t}$. The behavior of numerical solutions is similar to the previous two-dimensional results and is in good agreement to the exact solution under the motion by mean curvature.

3.4. Image segmentation

Now, we consider an image segmentation problem for the application of the AC equation. Let $\mathbf{x} = (x, y)$ be the two-dimensional coordinate. The geometric active contour model based on the mean curvature motion is given by the following evolution equation [33]:

$$\frac{\partial \phi(\mathbf{x}, t)}{\partial t} = g(f_0(\mathbf{x})) \left(-\frac{F'(\phi(\mathbf{x}, t))}{\epsilon^2} + \Delta \phi(\mathbf{x}, t) \right) + \beta g(f_0(\mathbf{x})) F(\phi(\mathbf{x}, t)). \tag{6}$$

Here, $f_0(\mathbf{x}) = (f(\mathbf{x}) - f_{\min}) / (f_{\max} - f_{\min})$, where f_{\max} and f_{\min} are the maximum and minimum values of the given slice image $f(\mathbf{x})$, respectively. And $g(f_0(\mathbf{x})) = 1 / [1 + |\nabla(G_\sigma * f_0)(\mathbf{x})|^2]$ is the edge stopping function which acts to stop the evolution when the contour reaches the edge, where $(G_\sigma * f_0)(\mathbf{x}) = \int_\Omega G_\sigma(\mathbf{x} - \mathbf{y}) f_0(\mathbf{y}) d\mathbf{y}$ is the convolution of the given image f_0 with the Gaussian function $G_\sigma(\mathbf{x}) = \frac{1}{2\pi\sigma^2} e^{-\frac{x^2+y^2}{2\sigma^2}}$. Also, free energy $F(\phi)$ is given as $F(\phi) = 0.25(\phi^2 - 1)^2$, and ϵ is a constant which is related to the phase transition width.

Fig. 5 illustrates the basic process of the image segmentation using Eq. (6). In this test, we use $\sigma = 1.5$, $\beta = 5e4$, ϵ_8 , $h = 0.01$, $\Delta t = 0.2h^2$, and 71×67 mesh grid. With a given medical image, which is obtained in Ref. [33], we define the scaled image $f_0(\mathbf{x})$ and initialize $\phi(\mathbf{x}, 0)$ as $\phi(\mathbf{x}, 0) = 1$ if \mathbf{x} is inside the square contour and $\phi(\mathbf{x}, 0) = -1$ otherwise (see Fig. 5(a)). As shown in Fig. 5(b) and (c), the initial data evolves until it reaches the boundary of the image through the motion by mean curvature and extra term in Eq. (6). Note that the extra term $\beta g(f_0(\mathbf{x})) F(\phi(\mathbf{x}, t))$ makes the contour evolve beyond the non-convex and disconnected regions. For more details, please refer to [33].

3.5. Crystal growth

Simulation of crystal growth processes has been of growing interest because of its importance in many technological applications [34]. We consider the solidification of a pure substance from its supercooled melt in both two- and three-dimensional spaces. Let us introduce an order parameter ϕ which is 1 in the solid phase and -1 in the liquid phase. The interface is defined by $\phi = 0$. The governing equations are given as

$$\begin{aligned} \epsilon^2(\phi) \frac{\partial \phi}{\partial t} &= \nabla \cdot (\epsilon^2(\phi) \nabla \phi) + [\phi - \lambda U(1 - \phi^2)](1 - \phi^2) \\ &\quad + \left(|\nabla \phi|^2 \epsilon(\phi) \frac{\partial \epsilon(\phi)}{\partial \phi_x} \right)_x + \left(|\nabla \phi|^2 \epsilon(\phi) \frac{\partial \epsilon(\phi)}{\partial \phi_y} \right)_y, \end{aligned} \tag{7}$$

$$\frac{\partial U}{\partial t} = D \Delta U + \frac{1}{2} \frac{\partial \phi}{\partial t}, \tag{8}$$

where $\epsilon(\phi)$ is the anisotropic function, λ is the dimensionless coupling parameter, and U is the dimensionless temperature field. For the four-fold symmetry, $\epsilon(\phi)$ is defined as

$$\epsilon(\phi) = (1 - 3\delta_4) \left(1 + \frac{4\delta_4}{1 - 3\delta_4} \frac{\phi_x^4 + \phi_y^4}{|\nabla \phi|^4} \right).$$

Here, δ_4 is a parameter for the anisotropy of interfacial energy. If $\delta_4 = 0$, then Eq. (7) becomes an Allen–Cahn type equation. Therefore, we can apply the proposed explicit hybrid scheme. We propose the following operator splitting scheme for Eqs. (7) and (8): First, we solve the part of Eq. (7) as

$$\begin{aligned} \epsilon^2(\phi_{ij}^n) \frac{\phi_{ij}^* - \phi_{ij}^n}{\Delta t} &= [\nabla \cdot (\epsilon^2(\phi) \nabla \phi)]_{ij}^n - \lambda U_{ij}^n (1 - (\phi_{ij}^n)^2)^2 \\ &\quad + \left[\left(\frac{16\delta_4 \epsilon(\phi) \phi_x (\phi_x^2 \phi_y^2 - \phi_y^4)}{|\nabla \phi|^4} \right)_{x,ij} \right]^n + \left[\left(\frac{16\delta_4 \epsilon(\phi) \phi_y (\phi_x^2 \phi_y^2 - \phi_x^4)}{|\nabla \phi|^4} \right)_{y,ij} \right]^n, \end{aligned}$$

where

$$\begin{aligned} &[\nabla \cdot (\epsilon^2(\phi) \nabla \phi)]_{ij} \\ &= \frac{\epsilon^2(\phi_{i+1,j}) + \epsilon^2(\phi_{ij})}{2h^2} (\phi_{i+1,j} - \phi_{ij}) - \frac{\epsilon^2(\phi_{ij}) + \epsilon^2(\phi_{i-1,j})}{2h^2} (\phi_{ij} - \phi_{i-1,j}) \\ &\quad + \frac{\epsilon^2(\phi_{i,j+1}) + \epsilon^2(\phi_{ij})}{2h^2} (\phi_{i,j+1} - \phi_{ij}) - \frac{\epsilon^2(\phi_{ij}) + \epsilon^2(\phi_{i,j-1})}{2h^2} (\phi_{ij} - \phi_{i,j-1}). \end{aligned}$$

Because the remaining of Eq. (7) is an ordinary differential equation, we solve it analytically and the closed-form solution is given as

$$\phi_{ij}^{n+1} = \phi_{ij}^* / \sqrt{e^{-\frac{2\Delta t}{\epsilon^2(\phi_{ij}^n)}} + (\phi_{ij}^*)^2 \left(1 - e^{-\frac{2\Delta t}{\epsilon^2(\phi_{ij}^n)}} \right)}.$$

Next, we use the explicit Euler method for Eq. (8):

$$\frac{U_{ij}^{n+1} - U_{ij}^n}{\Delta t} = D \Delta_d U_{ij}^n + \frac{\phi_{ij}^{n+1} - \phi_{ij}^n}{2\Delta t},$$

where we have used the standard five point stencil for the discrete Laplacian operator, i.e., $\Delta_d U_{ij} = (U_{i-1,j} + U_{i+1,j} - 4U_{ij} + U_{i,j-1} + U_{i,j+1})/h^2$.

In the two-dimensional simulation, a 512×512 mesh is used on the computational domain $\Omega = (-200, 200)^2$. We take the initial state as

$$\phi(x, y, 0) = \tanh \left(\frac{5 - \sqrt{x^2 + y^2}}{\sqrt{2}} \right) \quad \text{and} \quad U(x, y, 0) = \begin{cases} 0 & \text{if } \phi > 0 \\ \Delta & \text{else.} \end{cases}$$

We take $\Delta = -0.55$, $\delta_4 = 0.05$, and apply the homogeneous Neumann boundary conditions. The calculations are run up to time $T = 2000h^2$. To show the efficiency of the proposed scheme, we compare the numerical results with the explicit and implicit hybrid methods at several times. Here, we use the implicit hybrid method which is proposed in Ref. [35].

Fig. 6 represents the temporal evolution of crystal growth at $t = 800h^2$, $1200h^2$, $1600h^2$, and $2000h^2$. Here, EH and IH are the abbreviations of the explicit hybrid and implicit hybrid methods, respectively. From Fig. 6, results from the implicit hybrid method except $\Delta t = 0.05h^2$ case show large gaps compared with the proposed explicit hybrid method with $\Delta t = 0.05h^2$.

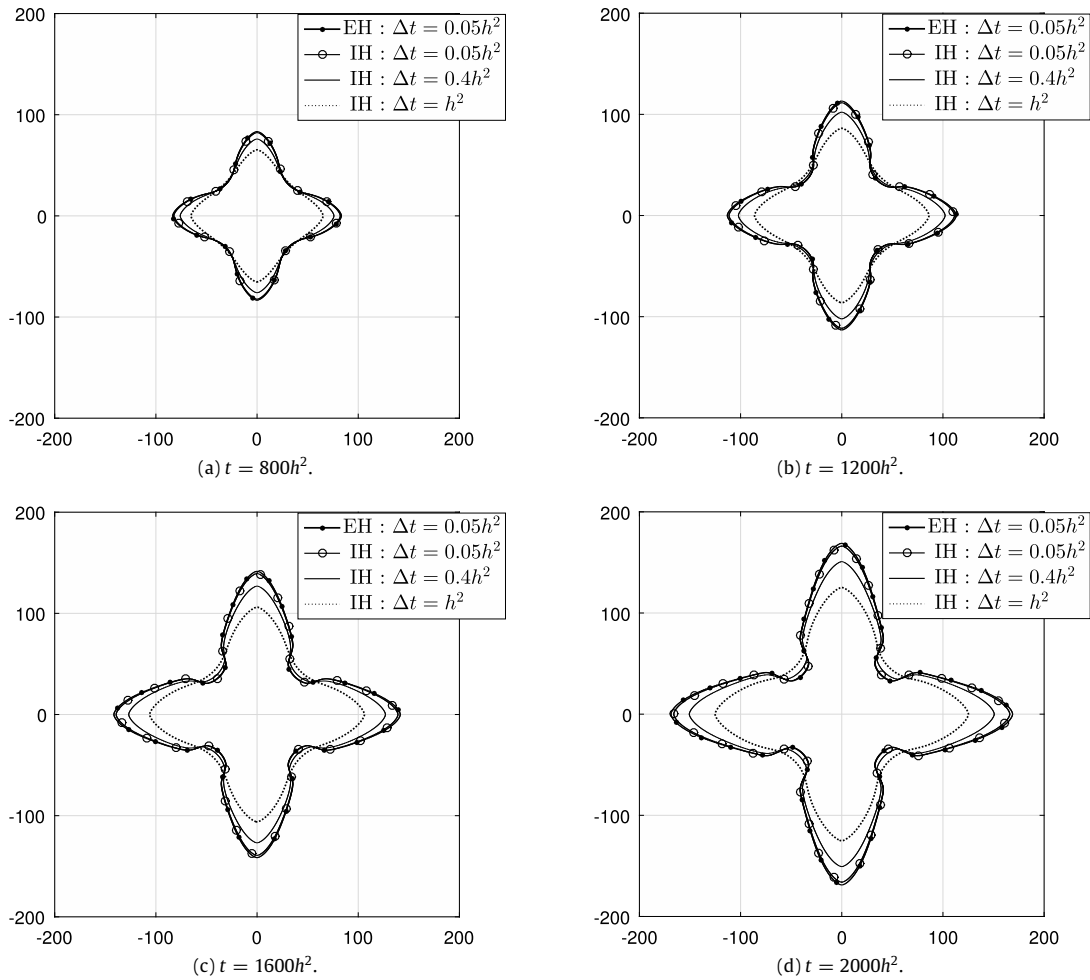


Fig. 6. Comparison of two-dimensional crystal growth by the proposed explicit hybrid and the previous implicit hybrid methods. Here, EH and IH denote the explicit hybrid and implicit hybrid methods, respectively.

Table 1

Relative CPU time of the implicit hybrid method with time step Δt_{im} . Here, $\Delta t_{ex} = 0.05h^2$ is used.

Time step (Δt_{im})	Δt_{ex}	$2\Delta t_{ex}$	$4\Delta t_{ex}$	$8\Delta t_{ex}$	$10\Delta t_{ex}$	$20\Delta t_{ex}$
Relative CPU time	5.6638	2.9203	1.6194	0.9634	0.8025	0.4458

Table 1 represents the relative CPU time of the implicit hybrid method with respect to time step size Δt_{im} to the explicit hybrid method with $\Delta t_{ex} = 0.05h^2$. For a similar CPU time, for example, the case with $\Delta t_{im} = 8\Delta t_{ex}$, the result with the explicit hybrid method is more accurate than that of the implicit hybrid method as shown in Fig. 6.

Next, we consider a three-dimensional crystal growth. The initial conditions are given as follows.

$$\phi(x, y, z, 0) = \tanh\left(\frac{5 - \sqrt{x^2 + y^2 + z^2}}{\sqrt{2}}\right), \quad U(x, y, z, 0) = \begin{cases} 0 & \text{if } \phi > 0, \\ \Delta & \text{else} \end{cases}$$

on the domain $\Omega = (-100, 100)^3$ with a mesh grid $256 \times 256 \times 256$. We take the same values as in the two-dimensional test for the other parameters. The calculations are run up to time $T = 600$.

Fig. 7(a) and (b) show evolutions of the interface with the previous implicit hybrid method ($\Delta t = 0.25h^2$) and the proposed explicit hybrid method ($\Delta t = 0.025h^2$), respectively. The CPU time takes about twice more than the previous implicit hybrid method. However, as shown in Fig. 7, numerical results by the previous method are not accurate compared to the proposed one. Therefore, to get an accuracy numerical result, we have to use a small enough time step size. In that case, it is better to use the proposed explicit hybrid method. Table 2 lists the relative CPU time of the implicit hybrid method and we get the similar CPU time results as with two-dimensional case.

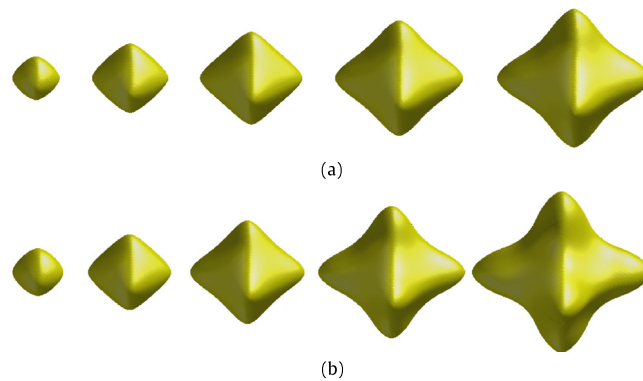


Fig. 7. Temporal evolution of three-dimensional crystal growth with (a) the previous implicit hybrid method ($\Delta t = 0.25h^2$) and (b) the proposed explicit hybrid method ($\Delta t = 0.025h^2$), respectively.

Table 2

Relative CPU time of the implicit hybrid method. Here, $\Delta t_{\text{ex}} = 0.025h^2$ is used.

Time step (Δt_{im})	Δt_{ex}	$2\Delta t_{\text{ex}}$	$4\Delta t_{\text{ex}}$	$8\Delta t_{\text{ex}}$	$10\Delta t_{\text{ex}}$	$20\Delta t_{\text{ex}}$
Relative CPU time	3.2006	1.8657	1.1686	0.6349	0.5167	0.3061

4. Conclusions

In this paper, we presented an explicit hybrid numerical method for the Allen–Cahn equation. To get an accurate numerical solution, we need to use a small enough time step size. In that sense, it is better to choose a fully explicit scheme for a numerical method. Therefore, we proposed the new numerical approach with the explicit scheme and splitting method for accuracy and efficiency. We showed the stability condition of the proposed numerical scheme and the pointwise boundedness of the numerical solution under a solvability condition. We carried out several numerical experiments such as linear stability analysis, traveling wave, motion by mean curvature, image segmentation, and crystal growth. By various numerical tests, we showed that the new numerical method is accurate and efficient.

Acknowledgments

The first author (D. Jeong) was supported by the National Research Foundation of Korea (NRF) grant funded by the Korea government (MSIP) (NRF-2017R1E1A1A03070953). The corresponding author (Junseok Kim) was supported by Basic Science Research Program through the National Research Foundation of Korea (NRF) funded by the Ministry of Education (NRF-2016R1D1A1B03933243). The authors greatly appreciate the reviewers for their constructive comments and suggestions, which have improved the quality of this paper.

References

- [1] S.M. Allen, J.W. Cahn, A microscopic theory for antiphase boundary motion and its application to antiphase domain coarsening, *Acta Metall.* 27 (6) (1979) 1085–1095.
- [2] A.A. Wheeler, W.J. Boettinger, G.B. McFadden, Phase-field model for isothermal phase transitions in binary alloys, *Phys. Rev. A* 45 (10) (1992) 7424–7439.
- [3] Y. Li, D. Jeong, J.I. Choi, S. Lee, J. Kim, Fast local image inpainting based on the Allen–Cahn model, *Digit. Signal Process.* 37 (2015) 65–74.
- [4] M. Beneš, V. Chaloupecký, K. Mikula, Geometrical image segmentation by the Allen–Cahn equation, *Appl. Numer. Math.* 51 (2–3) (2004) 187–205.
- [5] Y. Li, J. Kim, An unconditionally stable hybrid method for image segmentation, *Appl. Numer. Math.* 82 (2014) 32–43.
- [6] X. Feng, A. Prohl, Numerical analysis of the Allen–Cahn equation and approximation for mean curvature flows, *Numer. Math.* 94 (1) (2003) 33–65.
- [7] X. Feng, Y. Li, Analysis of symmetric interior penalty discontinuous Galerkin methods for the Allen–Cahn equation and the mean curvature flow, *IMA J. Numer. Anal.* 33 (4) (2013) 1–30.
- [8] C. Liu, J. Shen, A phase field model for the mixture of two incompressible fluids and its approximation by a Fourier-spectral method, *Physica D* 179 (3) (2003) 211–228.
- [9] D. Jeong, J. Kim, Conservative Allen–Cahn–Navier–Stokes system for incompressible two-phase fluid flows, *Comput. & Fluids* 156 (2017) 239–246.
- [10] H.D. Ceniceros, C.J. García-Cervera, A new approach for the numerical solution of diffusion equations with variable and degenerate mobility, *J. Comput. Phys.* 246 (1) (2013) 1–10.
- [11] D.J. Eyre, An unconditionally stable one-step scheme for gradient systems. Unpublished article (1998) <http://www.math.utah.edu/~eyre/research/methods/stable.ps>.
- [12] X. Feng, H. Song, T. Tang, J. Yang, Nonlinear stability of the implicit-explicit methods for the Allen–Cahn equation, *Inverse Probl. Imaging* 7 (3) (2013) 679–695.
- [13] C. Graäser, R. Kornhuber, U. Sack, Time discretizations of anisotropic Allen–Cahn equations, *IMA J. Numer. Anal.* 33 (4) (2013) 1226–1244.

- [14] F. Guillèn-González, G. Tierra, Second order schemes and time-step adaptivity for Allen–Cahn and Cahn–Hilliard models, *Comput. Math. Appl.* 68 (8) (2014) 821–846.
- [15] J. Kim, S. Lee, Y. Choi, A conservative Allen–Cahn equation with a space–time dependent Lagrange multiplier, *Internat. J. Engrg. Sci.* 84 (2014) 11–17.
- [16] S. Zhai, Z. Weng, X. Feng, Investigations on several numerical methods for the non-local Allen–Cahn equation, *Int. J. Heat Mass Transfer* 87 (2015) 111–118.
- [17] S. Zhai, Z. Weng, X. Feng, Fast explicit operator splitting method and time-step adaptivity for fractional non-local Allen–Cahn model, *Appl. Math. Model.* 40 (2) (2015) 1315–1324.
- [18] H.G. Lee, J. Kim, An efficient and accurate numerical algorithm for the vector-valued Allen–Cahn equations, *Comput. Phys. Comm.* 183 (10) (2012) 2107–2115.
- [19] H.G. Lee, J.Y. Lee, A semi-analytical Fourier spectral method for the Allen–Cahn equation, *Comput. Math. Appl.* 68 (3) (2014) 174–184.
- [20] F. Liu, J. Shen, Stabilized semi-implicit spectral deferred correction methods for Allen–Cahn and Cahn–Hilliard equations, *Math. Methods Appl. Sci.* (2013). <http://dx.doi.org/10.1002/mma.2869>.
- [21] D.F. Martin, P. Colella, M. Anghel, F.J. Alexander, Adaptive mesh refinement for multiscale nonequilibrium, *Phys. Comput. Sci. Eng.* 7 (3) (2005) 24–31.
- [22] J. Shin, S.K. Park, J. Kim, A hybrid FEM for solving the Allen–Cahn equation, *Appl. Math. Comput.* 244 (2014) 606–612.
- [23] S. Zhai, X. Feng, Y. He, Numerical simulation of three dimensional Allen–Cahn equation by high-order compact ADI method, *Comput. Phys. Comm.* 185 (10) (2014) 2449–2455.
- [24] X. Yang, Error analysis of stabilized semi-implicit method of Allen–Cahn equation, *Discrete Contin. Dyn. Syst. B* 11 (4) (2009) 1057–1070.
- [25] J.W. Choi, H.G. Lee, D. Jeong, J. Kim, An unconditionally gradient stable numerical method for solving the Allen–Cahn equation, *Physica A* 338 (9) (2009) 1791–1803.
- [26] Y. Li, H.G. Lee, D. Jeong, J. Kim, An unconditionally stable hybrid numerical method for solving the Allen–Cahn equation, *Comput. Math. Appl.* 60 (6) (2010) 1591–1606.
- [27] H.G. Lee, J.-Y. Lee, A second order operator splitting method for Allen–Cahn type equations with nonlinear source terms, *Physica A* 432 (15) (2015) 24–34.
- [28] L. Ju, J. Zhang, L. Zhu, Q. Du, Fast explicit integration factor methods for semilinear parabolic equations, *J. Sci. Comput.* 62 (2) (2015) 431–455.
- [29] A.A. Aderogba, M. Chapwanya, An explicit nonstandard finite difference scheme for the Allen–Cahn equation, *J. Difference Equ. Appl.* 21 (10) (2015) 875–886.
- [30] J.W. Thomas, *Numerical Partial Differential Equations: Finite Difference Methods*, Vol. 22, Springer Science & Business Media, New York, 2013.
- [31] S. Gadkari, R. Thaokar, Stability of immersed viscous liquid threads under electric field, *Internat. J. Engrg. Sci.* 62 (2013) 9–21.
- [32] A.M. Wazwaz, The tanh-coth method for solitons and kink solutions for nonlinear parabolic equations, *Appl. Math. Comput.* 188 (2) (2007) 1467–1475.
- [33] Y. Li, J. Kim, A fast and accurate numerical method for medical image segmentation, *J. KSIAM* 14 (4) (2010) 201–210.
- [34] L. Tan, N. Zabarar, A level set simulation of dendritic solidification of multi-component alloys, *J. Comput. Phys.* 221 (1) (2007) 9–40.
- [35] Y. Li, H.G. Lee, J. Kim, A fast, robust, and accurate operator splitting method for phase-field simulations of crystal growth, *J. Cryst. Growth* 321 (1) (2011) 176–182.